Main-chain nematic side-chain smectic composite liquid crystalline elastomers

*Hongye Guo Mohand O. Saed Eugene M. Terentjev**

Hongye Guo, Dr. Mohand O. Saed, Prof. Eugene M. Terentjev
Cavendish Laboratory, University of Cambridge, JJ Thomson Avenue, Cambridge, CB3 0HE, U.K
emt1000@cam.ac.uk

Keywords: *Liquid crystalline elastomers, Composites, Nematic, Smectic, Elasticity, Ductility*

A composite liquid crystalline elastomer is designed, combining main-chain and side-chain mesogenic polymers in the network, and resulting in micro-phase separated regions of nematic and smectic ordering in the macroscopically homogeneous elastomer. A range of different fractions of the components is explored, from fully nematic main-chain system, across to fully smectic side-chain elastomer. Thermal phase transitions of both phases coexisting in the material are detected by calorimetry, and the nematic/smectic structure investigated by X-ray scattering. The tensile stress-strain data reveals the key effect of such a multi-phase composite, where the nematic fraction adds ductility while the smectic fraction increases the modulus and mechanical stiffness. Varying the composition, we were able to optimize the mechanical properties of this material type.

1 Introduction

In liquid crystalline polymers (LCEs), a mono-functional mesogenic group can attach to the polymer backbone either head on, or side on, or alternatively – a di-functional mesogenic group can form the backbone chain itself, when separated by flexible spacers. In the former case, the mesogen ends up as a "side chain" pendant group, while in the latter case mesogens become a part of the polymer "main chain".
The first LCE materials had the side chain configuration, with the most prominent example being the polysiloxane LCEs of Finkelmann [1, 2]. Over the years, many other types of both main chain and side chain LCE networks have been explored. Owing to the exceptional physical characteristics of LCE, such as thermal actuation [3, 4, 5] and its "soft elasticity' '[6, 7], this field has become a focus of many disciplines, from physicists analyzing complex interaction between orientational order and rubber elasticity, to chemists developing novel synthesis procedures, to engineers looking for practical applications such as artificial muscles [8], smart textiles [9], sensors [10] and in soft robotics [11].
LCEs can also be categorized by their mesophases, mainly nematic and smectic. While most studies were focusing on the nematic, smectic LCE has also been interesting and important, both from experimental standpoint, offering several unique properties and characteristics [12, 13, 14, 15], and from theoretical angle, due to their distinct coupling between network crosslinks and the smectic layers [16, 17, 18].
Following in the footsteps of Finkelmann, most of the early LCEs were synthesized by the hydrosilylation reaction between the mesogenic units and the siloxane backbone (resulting in a side-chain configuration). However, the challenging nature of such synthesis route (temperature and humidity sensitive, prone to catalyst poisoning) slowed down the research progress. The most prominent main-chain LCE of that time was also obtained through a multi-step challenging synthesis[19, 20]. However, with the introduction of 'click' chemistry of thiol-enes and thiol-acrylates after a breakthrough in LCE chemistry in 2015 [21], most LCEs have now become main-chain, utilizing commercially available di-acrylate reacting mesogens as well as the much more robust reaction route. In contrast to the many significant advances with these new LCE materials[22, 23], the use of siloxane groups in LCEs has become less frequent. This is unfortunate, since siloxane groups still provide unparalleled advantages, leading to the significantly lower glass transition and some excellent mechanical properties [24]. Also, it was recently found that the siloxane segments allow for the dynamic bond exchange [25, 26], thus offering an opportunity for plastic re-moulding of siloxane LCEs, similar to vitrimers [27].
With such a broad range of properties, it is attractive to combine different distinct materials to produce composite LCEs. Making LCE composites has been tried in various ways, e.g. by doping the polymer network with foreign species [28], or by co-polymerization with non-LC monomers [29, 30]. Recently, the

concept of double networks has been tested to produce highly durable and tough LCE materials [31, 32]. In all cases, the aim was to enhance existing properties or even impart new physical properties, such as using nano-particles to promote fast response times and sensitivity to multiple stimuli, and use hydrogen bonding to increase strength and promote self-healing.
Composite LCEs can also be synthesized with multiple mesogenic species and network structures. By combining both smectic and nematic mesogens in the side chain formation, the presence and transition temperatures of certain phases could be manipulated [33]. When linking both long mesogenic oligomers and side chain mesogens (both nematic) to polymer backbones, one could obtain composite LCEs with exceptional thermal-mechanical properties [4, 34]. In this work, we extend this concept by combining previously studied smectic side-chain and nematic main-chain LCEs in one homogeneously crosslinked network, using the thiol-acrylate Michael addition click reaction. By adjusting the composition, the length of main chain oligomers and the frequency of attachment onto the siloxane backbone could be altered. thus controlling the overall weight fraction of nematic and smectic components of the composite. The resulting composite LCEs networks combine the excellent ductility offered by the main-chain nematic polymers, and the great mechanical strength originated from the layer constraints of the side-chain smectic phases.

2 Results and discussion

Strictly speaking, the cross-linking density in a polymer network is defined as the number of "cross-links" per unit volume. In a simple network of polymer chains with idealized 'point' crosslinkers, the crosslinking density is also related to the (inverse of) average volume of network strand. This parameter is closely tied to the rubber elastic modulus, although the chain entanglements [35] also contribute to the mechanical strength. In many studies regarding LCEs however, the cross-linking density normally describes the molar ratio of the cross-linking reaction groups to reaction groups on the monomers (for main chain LCEs) and the backbones (for side chain LCEs). When combining long oligomers as crosslinkers, side chain mesogens and a polymer backbone, the idealized format of crosslinking density is no longer applicable. One could regard the ultimate 3-functional bond as the point crosslinker, but then there are very different polymer chains linking into the network, and certainly none of the simple scalar parameters such as "cross-linking density" have any meaning. Thus in this study, a different naming system with a format of x-y was applied to reflect the network composition, as shown in **Table 1**. The first number represents the average number of side-chain mesogenic units between connections to the main-chain oligomers, while the second number gives the average number of mesogens in each linear oligomer. In this nomenclature, the 'pure SC' elastomer crosslinked by just one diacrylate unit is (6-0) reflecting the simple 15% cross-linking density, while the 'pure MC' elastomer crosslinked by a a 4-functional thiol is (0-10) reflecting its simple 10% cross-linking density.
Figure 1 illustrates the synthesis procedure for composite LCEs. We used two steps of thiol-acrylate click chemistry. The first step is to produce a stock of main-chain oligomer "cross-linker" of controlled

Sample	N_{SC}	N_{MC}	MC wt%	T_g [C]	T_{SI}[C]	T_{NI}[C]
Pure SC	6	0	0%	-12	52	–
6-5	6	5	39.8%	-10	52	38
6-10	6	10	56.9%	-10	48	38
3-5	3	5	55.4%	-10	52	38
3-10	3	10	71.4%	-5	53	38
Pure MC	0	10	100%	-2	–	38

Table 1: The summary and comparison of molecular compositions and thermal transitions in the composite LCE networks. The 'Pure SC' material is the 15%-crosslinked chain LCE [36], the 'Pure MC' is the 10%-crosslinked main-chain LCE [23]. The four examples of composite network between these two limits are ranked by the increasing weight fraction of the main-chain nematic polymer, as indicated in the 4th column of the table. Temperatures of transitions are obtained from the DSC data in Fig. 2.

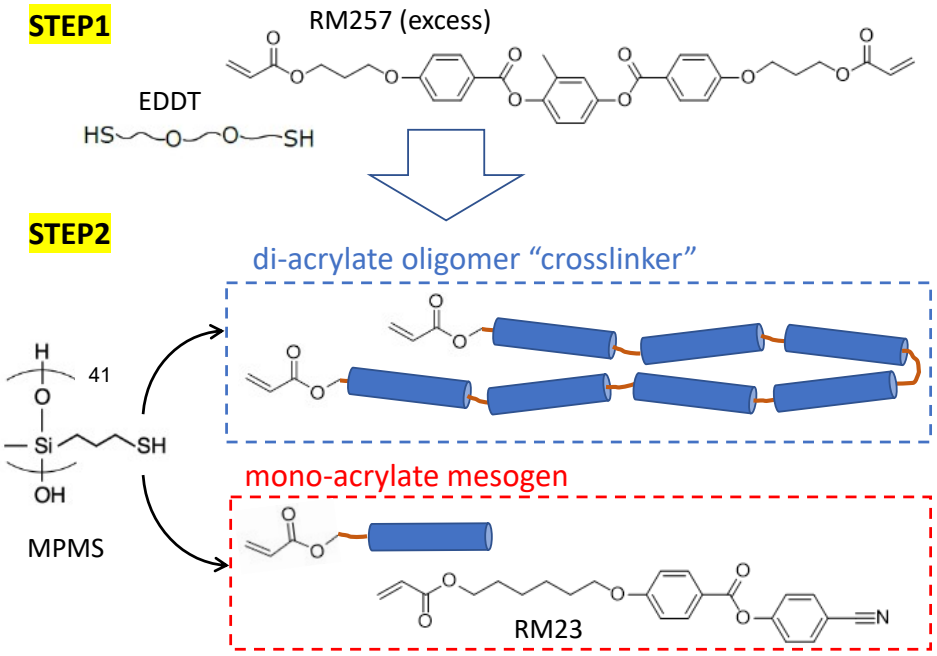

Figure 1: Chemical structures of main-chain side-chain LCE constituents: The polysiloxane backbone polymer chain with thiol functional groups (MPMS), with the average chain length $n = 41$ (molecular weight 4000-7000 g/mol); side-chain acrylate reacting mesogens RM23; the di-acrylate oligomer crosslinker prepared with di-acrylate mesogens RM257 and di-thiols EDDT. The thiol functional groups on MPMS react with acrylate groups on both the mono-acrylate mesogen and the oligomer to form a complete network.

chain length, terminated with acrylate groups at the ends (which is achieved by varying the excess of di-acrylates over di-thiols in this step of the reaction, see Experimental Details below). At the second step, a mixture of di-acrylate oligomer and mono-acrylate mesogenic monomer was reacted with thiol-substituted siloxane chain to form the composite network. We were very aware of the big impact of conditions at the network formation step: since the Michael addition could be initiated at any temperature, we could produce the 'nematic genesis' LCEs by carrying out the Step-2 at ambient temperature in the nematic phase [37, 38]. In that case, the Schlieren texture of the nematic polymer melt would become crosslinked and form one set of internal constraints for the subsequent mechanical deformations. We could carry out the Step-2 at a high temperature, in the isotropic phase, thus forming 'isotropic-melt genesis' LCE network, in which randomly oriented crosslinks create the quenched disorder on cooling into the liquid-crystal state, resulting in the spin-glass polydomain structure and a different set of internal constraints [39]. In both these methods, one also inevitably forms the chain entanglements (starting from the dense melt of chains), and after crosslinking, these entanglements become permanently frozen, strongly affecting the mechanical response and ductility [35].
For these reasons, we have chosen to produce the LCE networks of 'isotropic-solution' genesis, that is have at least 50% solvent at the Step-2 of the reaction. In this case, the material is isotropic, but also – the crosslinked chains are stretched and not entangled. On subsequent de-swelling, the network compacts into the dense elastomer, but the entanglements cannot form since there are no free dangling ends after cross-linking. There is a large literature suggesting that this is the most 'clean' LCE system, both for its phase transitions and its mechanical response to deformation.

2.1 Order and structure

The phase transformation behaviour of LCE samples is characterized by differential scanning calorimetry (DSC), with results shown in **Figure 2**. All samples went through three cycles of heating/cooling and the resulted DSC curves showed good reproducibility. On each cooling curve from the 4 composite LCEs, there are three main features: a step corresponding to the glass transition temperature T_g; a small peak at just below 40 degrees; and a much larger peak at a higher temperature. As these sam-

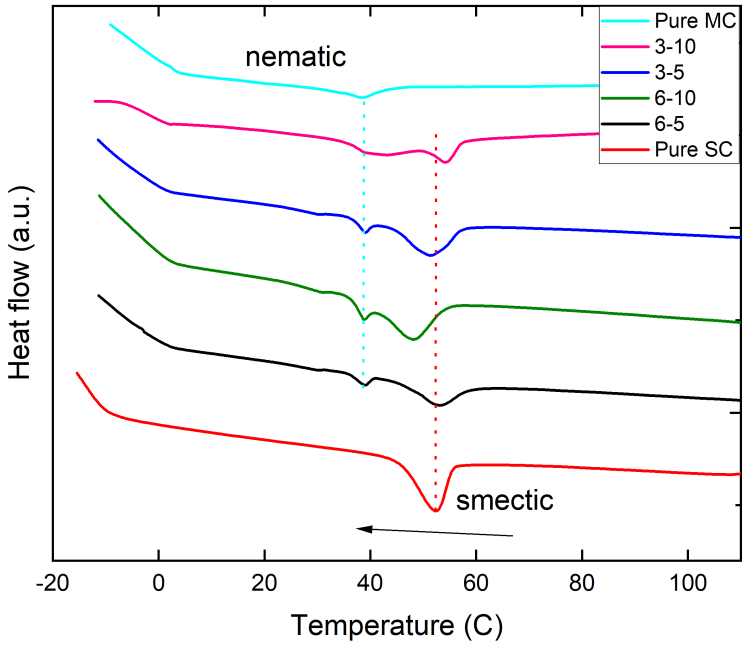

Figure 2: Differential scanning calorimetry data on cooling the composite LCE networks under study (the heating curves offer the same information). The dashed lines mark the correspondence of nematic and the smectic transitions in the composites to their pure-phase originals. The fact that the nematic transition occurs below smectic, is a strong evidence for micro-phase separation of nematic and smectic phases.

ples were synthesized with LCE mesogens known for their smectic side-chain and nematic main-chain propensity, one might assume the composite LCE to go through smectic-nematic-isotropic transitions sequence, and result in the two transition peaks in the DSC trace. However, the nematic to isotropic peak of pure main-chain LCE is of great similarity to the smaller peak (both in height and temperature), and we are forced to assume that the similar peaks in the four composite curves represent the nematic transition. Recall, that the nematic-isotropic is the so-called 'weak first order transition' [40, 41], e.g. in contrast to a much higher enthalpy of the smectic-isotropic transitions in the same plot. The smectic to isotropic peak of pure side-chain LCE is of great similarity to the larger peaks in the composite curves. In a homogeneous material, the smectic to nematic transition temperature T_{SN} must be lower than the nematic to isotropic transition temperature T_{NI}. This is not the case in our composite LCEs, which suggest the phase separation of nematic and smectic regions, each undergoing its own transition into the isotropic phase – but not between each other. However, the network is homogeneously crosslinked, and we have confirmed the full conversion of all reacting groups (see below, in Experimental Details), so we must be facing a micro-phase separation of different phases, as in copolymers.

To examine the network structure, X-ray analysis was performed at room temperature on all samples, first in the un-aligned polydomain state. Apart from pure main chain LCE10 (the known nematic material), all other XRD patterns contain both a nematic and a smectic ring, see **Figure 3**. Upon stretching, and therefore uniaxially aligning the samples, the nematic and smectic rings converge into bright spots orthogonal to each other, as is expected in these phases structure when the long axes of mesogens are parallel to the overall director and the stretching axis. The second–order diffraction peaks could also be seen for the aligned smectic case, confirming a strong layer separation. The differences between composite LCE samples in their XRD patterns were negligible.

In order to explain the observations above, a schematic drawing in **Figure 3(a,b)** proposes the structure of main-chain side-chain composite LCE network. In the natural polydomain states, the mono-acrylate smectic mesogens concentrate and form domains of layered smectic structure, strongly promoted by the

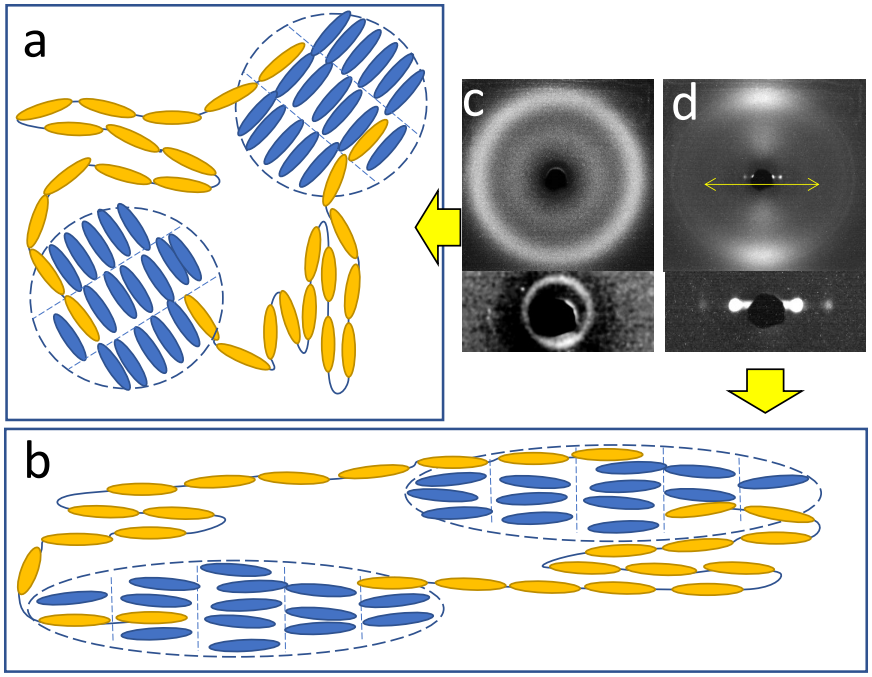

Figure 3: A schematic drawing of the nematic main-chain and smectic side-chain regions of the composite LCEs. (a) Polydomain samples with domains of smectic side chain LCEs interconnected by branches of nematic main chain oligomers. (b) Upon stretching, all domains (both nematic and smectic) first rotate to align their layer normal and mesogen director to the external stress. The "hair pins" structures found in main chain sections then starts to disappear. (c) & (d), XRD patterns corresponding to the polydomain (a) and monodomain (b) samples. The small angle patterns is placed under the wide angle patterns to reveal the hidden smectic signals blocked by the beam stop. The arrow in (d) indicates the direction of stretching.

poorly-miscible flexible siloxane backbone. The main-chain oligomers branch out from these smectic regions and link together to form regions of the nematic phase. The alignment direction of each smectic or nematic domains is randomly distributed, but upon applying an external stress, the nematic domains align, and smectic domains rotate and elongate as well, preserving the layer normal parallel to the direction of stretching.

It is important to try and determine the size of separated smectic domains. However, short of small-angle neutron scattering of deuterated siloxane segments (which we are not equipped to do), we see no way to determine this size. It cannot be less than ca. 10nm because this is the coherence length of liquid-crystalline phase to form, and it cannot be greater than a micron because we would then observe it under a microscope. Instead, the polarising microscopy shows a completely homogeneous structure on the optical length scale – but also a very unusual feature: when we uniaxially align the elastomer film by high stress (e.g. **Figure 3(d)**, one expects a typical uniaxial birefringence, like in all monodomain LCEs studied so far (nematic or smectic). Instead, we find the uniform light propagation at all orientations of crossed polarisers, with no noticeable variation with the angle of alignment, which tells that the aligned texture is not a simple uniaxial LCE: the presence of phase-separated regions gives enough scattering at all orientations. To confirm, when the films are heated into the isotropic phase, they become clear and absolutely transparent, meaning that no phase separation (i.e. demixing of siloxane from acrylate chains) occurs, and the composite structures we observe are formed due to the nematic/smectic phase mismatch.

It is important to emphasize that the discussed micro-phase separation must involve multiple network chains in each region: since our monomer count on each network strand is quite low (3, 6, or 10 units at most), this is not enough to form a 'phase' (neither nematic nor smectic) with such a distinct thermal and XRD signature. Topologically, this means that there are a lot of 'loops' in the network, which are the source of high ductility on mechanical stretching.

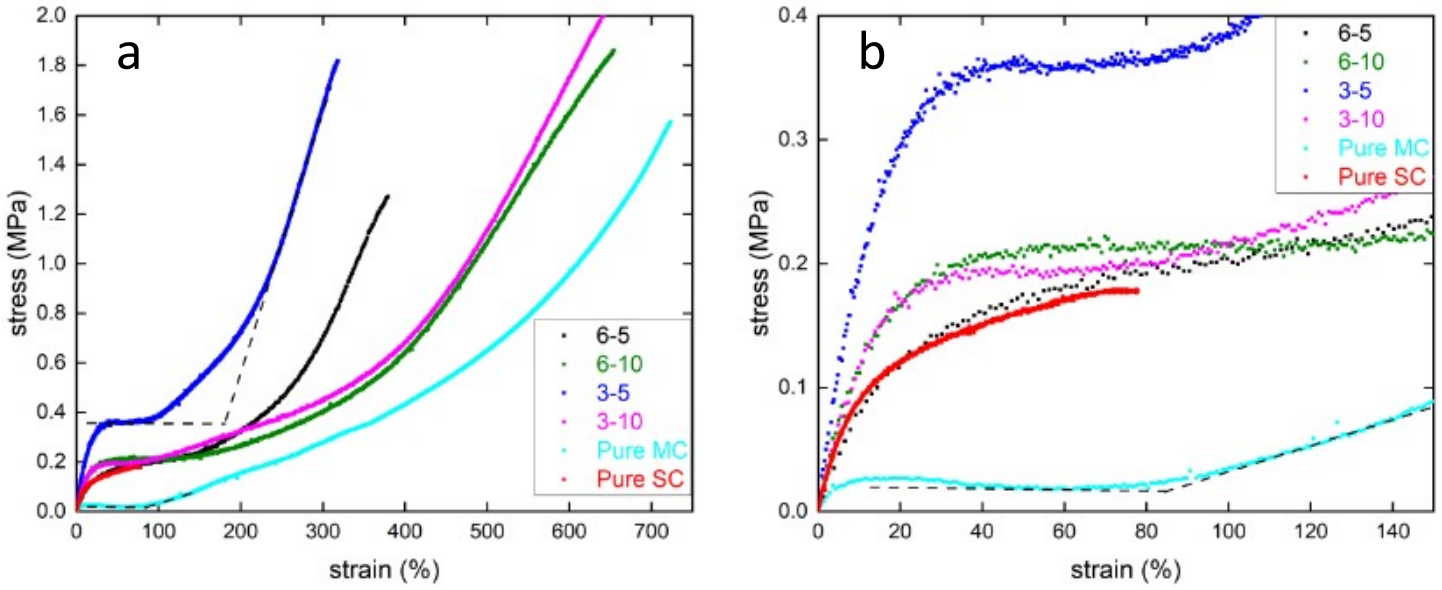

Figure 4: (a) Stress-strain curves for all four composite LCEs (black: 6-5, green: 6-10, blue: 3-5, pink: 3-10) as well as pure main chain and pure side chain LCEs (light blue: pure main chain LCE, red: pure side chain LCE). (b) To better compare samples' behaviours at low strain values, a magnified stress-strain plot is provided. The dashed lines in both (a) and (b) are used to locate ϵ_2.

2.2 Tensile stress-strain

The mechanical properties of our composite micro-phase separated LCEs were examined by tensile testing and compared with their matching pure main-chain and side-chain elastomers. The common practice in such tests in the LCE literature is using rectangular strips of samples; however, we found that this is an unreliable approach, especially when large tensile strains are of interest, because of the concentration of stress at the edges of constraining clamps. To address this effect and make the stress-strain data comparable and reproducible, we followed the industry standard of tensile testing and used dog-bone shaped samples (by reproducing the proportions of the ASTM D638 standard). In this way, we are assured that the clamping regions have no significant effect on the stress-strain curves, and accurately record the response at large tensile stress. The same applies to the rate of strain application, with different literature reports all having different strain rates. The industry standard (ASTM D638) was used again, of a strain rate of 0.25%/s in all tests, for reproducibility. The test results are shown in **Figure 4**.
All samples except the pure side chain RM23 sample exhibit the classical stress-strain response of polydomain LCEs (isotropic genesis): After the initial linear-elastic region (often called "semi-softness" in the literature), the material would strain at a constant level of stress plateau (onset at ϵ_1). Above ϵ_1, the elongation of the network is only caused by rotation of both nematic and smectic domains towards the direction of the external mechanical force. This alignment process terminates gradually as the network approaches the fully-aligned monodomain state, above which the stress-strain curve shows a modulus parallel to the director axis. However, unlike in the case of pure nematic LCE, one can see clearly that this alignment region is very diffuse, and any attempt to identify any specific strain ϵ_2 at which full alignment is achieved, is futile. This is explained by the internal micro-phase separated nature of the materials leading to another elongation mechanism: Once the nematic domains in the main chain sections are aligned, the network can still gain a lot of additional soft elongation by re-shaping the smectic domains.
For the pure nematic main-chain LCE (0-10), the characteristic low plateau is measured at only 0.02 MPa, and the semisoft onset ϵ_1 is only 3-5% strain. On the other side, the pure smectic side-chain LCE (6-0) would consistently break before reaching its stress plateau. This phenomenon was observed in the previous study ([36]) and is caused by the strong internal constraints of crosslinks within the layers. Judging by its trajectory, the level of stress plateau would be around 0.2 MPa. This serves as a "baseline"

above which all other composite LCE systems reside. In fact, samples 3-10, 6-5 and 6-10 all have their plateaus at around 0.2 MPa, similar to the pure side chain case. The semisoft onset ϵ_1 is also much higher, at 20-30% elongation, reflecting the strong influence of internal constraints.
Drawing attention to sample 3-5, its stress plateau stands out and reaches 0.36 MPa (with the onset strain ϵ_1 similar to other composites). This is caused by the much higher cross-linking density of this network, comparing to other systems. Another special case is the sample 6-5, with the most side-chain content among our composites. Its stress-strain response most closely resembles the pure side chain case, and instead of a flat stress plateau, it shows a noticeable slope with low modulus, suggesting a greater role of smectic layer constraints in the overall response.
In general, it appears that all composite elastomers eventually break at a tensile stress between 1.5 and 2MPa. There is a high variability of this breaking point, naturally as the crack initiation is a stochastic process, even in our tensile-optimized dog bones. This suggests that it is the nematic main-chain segments of the network that eventually undergo failure, when siloxane smectic domains are probably fully unwrapped at such high deformations.

3 Conclusion

By combining nematic main-chain oligomers and smectic-forming polysiloxane side-chain polymers, the mixed composite LCEs form a very unusual micro-phase separated internal structure. Calorimetry and X-ray analysis reveals the details of this phase separation and allows us to propose a model of network structure. In this model, we have micro-domains of smectic phase of aggregated side-chain siloxane, embedded into and interconnected by branches of nematic main chains. Deformation of this structure leads to the high ductility, and network toughness (defined as the integral under the stress-strain curve), compared with their pure smectic or nematic parent species. At the same time, their blocking stress that defines the soft or semi-soft plateau is increased by at least an order of magnitude due to the existence of smectic domains in the elastic matrix.
By varying the length of main-chain oligomers, and the density of attachments to the siloxane backbone during the crosslinking, we were able to scan a range of composition fractions, with the side-chain majority, equal, and main-chain majority systems. Each of these have distinct mechanical properties, which are determined by the relative sizes (and probably shapes) of smectic domains in the continuous matrix. Among various possible applications, such main-chain / side-chain micro-phase separated systems offer an improved mechanical strength and ductility of LCE actuators. However, to achieve that, further work must make sure that the monodomain alignment of uniaxial order is achieved, which could naturally occur in the popular 3D printing, or by using the plastic programming based on equilibrium siloxane bond exchange.

4 Experimental Section

Materials: Mono-acrylate mesogenic reacting monomer 4-methoxyphenyl 4-((6-(acryloyloxy) hexyl)oxy) benzoate (designated RM23 by the supplier) was purchased from Wilshire Technologies Inc. Di-acrylate mesogenic reacting monomer RM257 was purchased from Daken Chemical Co. As a commonly used reacting mesogen, RM257 could be sourced from many suppliers. The siloxane polymer backbone with thiol-substituted reacting side groups, (mercaptopropyl) methylsiloane (MPMS), was purchased from Gelest, Inc. 2,2'-(ethylenedioxy) diethanethiol (EDDT) was purchased from Sigma-Aldrich, as the flexible spacer for the synthesis of main chain oligomers. Toluene was purchased from Sigma-Aldrich. Dipropylamine (DPA) and Triethylamine (TEA) was purchased from Sigma-Aldrich and used as the catalyst for thiol-acrylate Michael addition reaction.

Synthesis procedure: In this work, a "two-steps reaction" route was taken to produce dog-bone shaped polydomain LCE samples in a Teflon mould.

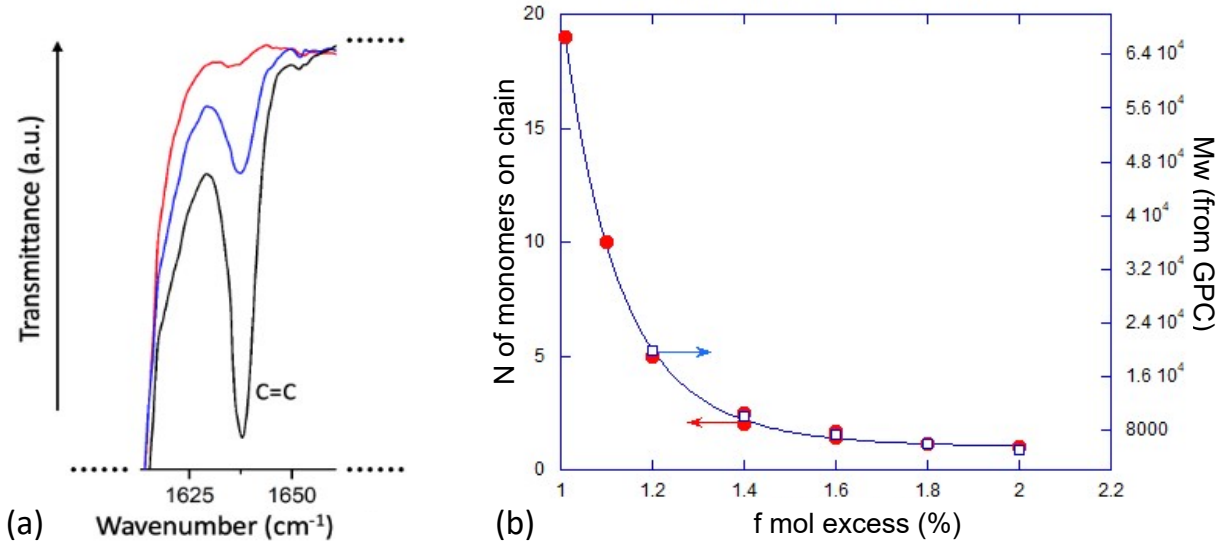

Figure 5: (a) Transmission peaks of C=C double bonds in the FTIR spectrum at different stages of reaction: start of reaction (black), 5 minutes into the reaction (blue) and red (3 hours after the onset of reaction). (b) Gel permeation chromatography (GPC) tests of oligomer synthesis. The blue line represents the theoretical calculation of chain length, while the red and blue data points were collected from acrylate excess and thiol excess oligomers respectively.

Step 1 (oligomer preparation): Excess amount of RM257 was dissolved in toluene (60 wt% relative to RM257) with EDDT in a vial assisted by gentle heating and vigorous mixing. Then, TEA (1 wt% relative to all components) was added and thoroughly mixed before being allowed to react for 24 hours at room temperature. Acrylate-terminated oligomers with 10 and 5 mesogenic monomers were prepared in this way by adjusting the molar ratio of RM257 and EDDT. To confirm the average length of oligomer chains, gel permeation chromatography (GPC) analysis was performed at various ratios of acrylate and thiol species, see **Figure 5**.
Step 2 (polymerization): Due to the significantly increased viscosity, the oligomer product was first diluted with additional toluene (the amount of diluting toluene was calculated to ensure a 80 wt% overall solvent content). In a separate vial, the mono-acrylate mesogen RM23 and the siloxane backbone MPMS were dissolved in toluene assisted by gentle heating and vigorous mixing. Contents in both vials were combined and mixed until homogeneous. By changing the amount of RM23 while ensuring 1:1 ratio of overall thiol (on the siloxane backbone) and acrylate (from both RM23 and oligomers), the average number of side chain segments between oligomer connections was adjusted. DPA catalyst was first diluted with toluene (5 times more) and then added into the main reaction vial. After vigorous mixing, the reaction mixture was degassed in a desiccator before pouring into a teflon mould. To prevent solvent evaporation, the mould was overfilled and covered with glass plate. After curing for 24 hours, the samples were removed from the mould and placed in a vacuum oven at 80 degrees for solvent removal.
Note that in the first step, a weaker catalyst TEA was used, instead of DPA, since a slower reaction is needed for more consistent oligomer chain lengths. The completion of such thiol-acrylate Michael addition reactions (specifically with thiols on siloxane backbones) was verified by monitoring the infrared spectrum (FTIR) of cross-linked samples (**Figure 5**).

Differential scanning calorimetry: Differential scanning calorimetry (DSC) was performed on all samples to study the phase transitions: we used a DSC4000 instrument from PerkinElmer. Samples were first heated to 100 °C to erase any effects of thermal history, followed by three cycles of cooling/heating between -20 and 120 °C, at a rate 10 °C/min with soak time of 2 minutes at each terminal temperature.

Wide- and small-angle X-ray scattering: Wide- and small-angle X-ray analysis were performed on all samples at room temperature using a Philips PW-1830 diffractometer with the main CuK_α wavelength of 0.154 nm. The data were collected by a wide-area detector (using 16.8 MP sCMOS GSense camera 67x67mm, from Photonic Science) at two sample-to-detector distances (112 and 68 mm) with an exposure time of 80 seconds. Data were gathered from samples with aligned monodomain texture to benefit

from the induced director alignment and have the distinct scattering patterns. The scattering patterns were processed and analysed by ImageJ.

Stress-strain tensile testing: Tensile tests were performed on all samples on a tensiometer ST1 from Tinius Olsen. The samples were moulded to be the standard dogbone shapes to avoid complications caused by the rigid clamp edges. The length of samples were determined by measuring the straight section in the middle. For our tests, this straight middle section was measured to have a dimension of 16 x 1.3 x 2.2 mm. Samples were loaded into the tensile machine by gluing each end (away from the straight section) onto a piece of solid plastic which was clamped by the machine, to avoid another complication of clamp compression damage. The samples were stretched at a strain rate of 0.253%/s.

Acknowledgements
H.G. acknowledges support from the China Scholarship Council. M.O.S. acknowledges support from the Royal Society via the University Research Fellowship. This work was funded by the European Reasearch Council (H2020) AdG No. 786659.

References

[1] H. Finkelmann, H.-J. Kock, G. Rehage, *Makromol. Chem. Rapid Comm.* **1981**, *2*, 4 317.

[2] J. Küpfer, H. Finkelmann, *Makromol. Chem. Rapid Comm.* **1991**, *12* 717.

[3] J. Küpfer, H. Finkelmann, *Macromol. Chem. Phys.* **1994**, *195* 1353.

[4] A. R. Tajbakhsh, E. M. Terentjev, *Eur. Phys. J. E* **2001**, *6* 181.

[5] M. Warner, *Annu. Rev. Condens. Matter Phys.* **2020**, *11* 125.

[6] M. Warner, P. Bladon, E. M. Terentjev, *J. Phys. II France* **1994**, *4* 93.

[7] P. D. Olmsted, *J. Phys. II France* **1994**, *4* 2215.

[8] D. J. Roach, C. Yuan, X. Kuang, V. C.-F. Li, P. Blake, M. L. Romero, I. Hammel, K. Yu, H. J. Qi, *ACS Appl. Mater. Interfaces* **2019**, *11*, 21 19514.

[9] T. Ohzono, M. O. Saed, Y. Yue, Y. Norikane, E. M. Terentjev, *Adv. Mater. Interfaces* **2020**, *7* 1901.

[10] C. Ohm, M. Brehmer, R. Zentel, *Adv. Mater.* **2010**, *22* 3366.

[11] A. Kotikian, C. McMahan, E. C. Davidson, J. M. Muhammad, R. D. Weeks, C. Daraio, J. A. Lewis, *Sci. Robot.* **2019**, *4* eaax7044.

[12] I. A. Rousseau, P. T. Mather, *J. Am. Chem. Soc.* **2003**, *125*, 50 15300.

[13] H. P. Patil, R. C. Hedden, *J. Polym. Sci. Part B: Polym. Phys.* **2007**, *45*, 24 3267.

[14] H. P. Patil, D. M. Lentz, R. C. Hedden, *Macromolecules* **2009**, *42*, 10 3525.

[15] Y. Nishimura, J. Chung, H. Muradyan, Z. Guan, *J. Am. Chem. Soc.* **2017**, *139* 14881.

[16] T. Lubensky, E. Terentjev, M. Warner, *J. Phys. II* **1994**, *4*, 9 1457.

[17] M. J. Osborne, E. M. Terentjev, *Phys. Rev. E* **2000**, *62* 5101.

[18] J. M. Adams, M. Warner, *Phys. Rev. E* **2005**, *71* 021708.

[19] V. Percec, M. Kawasumi, *Adv. Mater.* **1992**, *4* 572.

[20] V. Percec, M. Kawasumi, *Macromolecules* **1992**, *25* 3843.

[21] C. M. Yakacki, M. Saed, D. P. Nair, T. Gong, S. M. Reed, C. N. Bowman, *RSC Adv.* **2015**, *5* 18997.

[22] T. White, D. J. Broer, *Nat. Mater.* **2015**, *14* 1087.

[23] M. O. Saed, R. H. Volpe, N. A. Traugutt, R. Visvanathan, N. A. Clark, C. M. Yakacki, *Soft Matter* **2017**, *13* 7537.

[24] B. H. Jo, L. M. Van Lerberghe, K. M. Motsegood, D. J. Beebe, *J. Microelectromech. Syst.* **2000**, *9* 76.

[25] M. O. Saed, E. M. Terentjev, *Sci. Rep.* **2020**, *10*, 1 6609.

[26] Y. Wu, Y. Yang, X. Qian, Q. Chen, Y. Wei, Y. Ji, *Angew. Chem. Int. Ed* **2020**, *59* 4778.

[27] M. O. Saed, A. Gablier, E. M. Terentjev, *Chem. Rev.* **2022**, *122* 4927.

[28] Y. Ji, J. E. Marshall, E. M. Terentjev, *Polymers* **2012**, *4*, 1 316.

[29] S. Ahir, A. Tajbakhsh, E. Terentjev, *Adv. Funct. Mater.* **2006**, *16* 556.

[30] M. Yan, J. Tang, H. Xie, B. Ni, E. Zhang, H.and Chen, *J. Mater. Chem. C* **2015**, *3* 8526.

[31] M. Barnes, R. Verduzco, *Soft Matter* **2019**, *15* 870.

[32] X. Lin, W. Zou, E. M. Terentjev, *Macromolecules* **2022**, *55*, 3 810.

[33] V. Domenici, J. Milavec, A. Bubnov, D. Pociecha, B. Zupancic, A. Resetic, V. Hamplova, E. Gorecka, B. Zalar, *RSC Adv.* **2014**, *4* 44056.

[34] H. Wermter, H. Finkelmann, *e-Polymers* **2001**, *1*, 1 13.

[35] S. Kutter, E. M. Terentjev, *Eur. Phys. J. E* **2001**, *6* 221.

[36] H. Guo, M. O. Saed, E. M. Terentjev, *Soft Matter* **2022**, *18* 4803.

[37] H. Higaki, K. Urayama, T. Takigawa, *Macromol. Chem. Phys.* **2012**, *213* 1907.

[38] N. A. Traugutt, R. H. Volpe, M. S. Bollinger, M. O. Saed, A. H. Torbati, K. Yu, N. Dadivanyan, C. M. Yakacki, *Soft Matter* **2017**, *13* 7013.

[39] S. V. Fridrikh, E. M. Terentjev, *Phys. Rev. E* **1999**, *60* 1847.

[40] A. I. Larkin, S. A. Pikin, *Sov. Phys. JETP* **1969**, *29* 891.

[41] H. Yurtseven, *Phase Transitions* **1994**, *47* 59.

Table of Contents

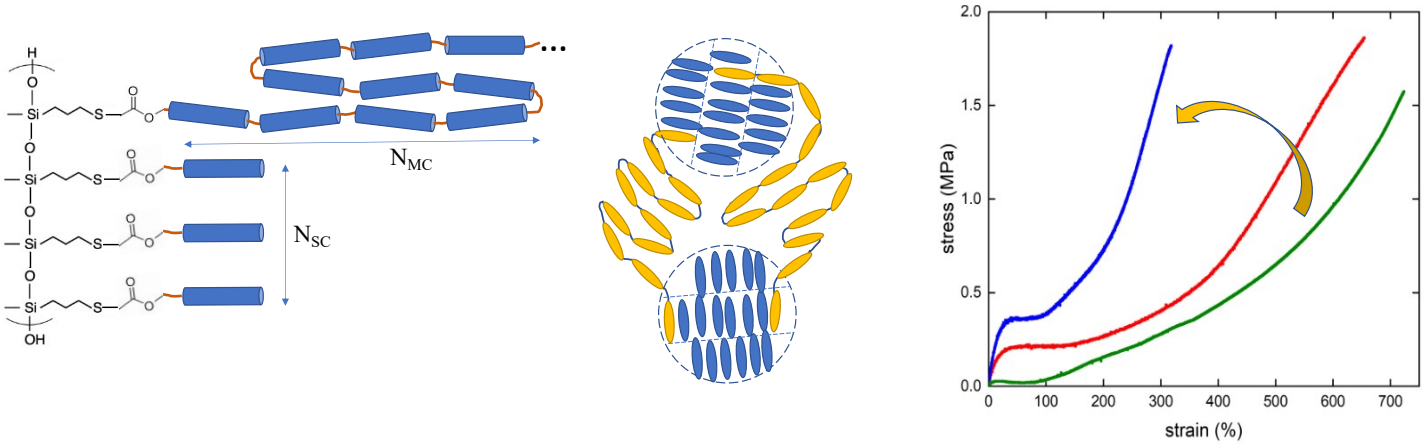

The composite liquid crystalline elastomers with the mixed main-chain / side-chain topology, using the siloxane backbone, were developed. We show that such composites break into micro-phase separated regions of nematic and smectic order, which leads to much improved mechanical properties of the network.